Influence of Near Fault Records on the Optimal Performance of Isolated Continuous Bridges

Influence of near fault records on the optimal performance of isolated continuous bridges

Elena Miceli[1][0000-0002-1262-3403]

[1] Politecnico di Torino, Corso Duca degli Abruzzi, 10129, Turin, Italy
elena.miceli@polito.it

Abstract. This study aims at evaluating the optimal value of the friction coefficient in case of multi-span continuous deck bridges equipped with single concave friction pendulum devices. The bridge is modelled with a six-degree-of-freedom system considering the presence of the isolator on top of both the abutment and the pier. The friction pendulum device behaviour is modelled by including the dependency of the friction coefficient on the velocity. The equation of motions have been solved by adopting a nondimensionalization with respect to the peak ground acceleration-to-velocity ratio, which is a measure for the ground motion period. A parametric analysis has been performed by using different values for the friction coefficient, for the pier and deck periods and the masses of the deck and of the pier. The uncertainty in the seismic input is included by considering 40 near fault records. Finally, an optimal value for the friction coefficient able to minimize the substructure peak response is calculated as function of the peak ground acceleration-to-velocity ratio and the period of the deck.

Keywords: continuous deck bridges, friction coefficient, optimal value.

1 Introduction

The seismic isolation is one of the largely adopted techniques to improve the seismic safety of civil structures [1]-[2]. In particular, the goal of the seismic isolation in case of bridges is to increase the period of the isolation system with the aim to reduce the inertia forces acting on the deck and subsequently transmitted to the substructure, i.e., the piers [3]. The advantage of using the friction pendulum systems (FPS) devices is to make the isolation period independent from the mass of the deck [4]-[5]. Big efforts have been made within the researchers to study how to model the FPS devices behaviour [6]-[10]. The existence of an optimal value of the friction coefficient, able to minimize the seismic response of the substructure, was first introduced by Jangid in [11]-[12]. To this aim, the optimal friction coefficient is evaluated in [13]-[14] through a parametric analysis (i.e., by varying many properties of the structure and the seismic input). However, in these works the optimization is not independent from the seismic input.

In this study, the optimal friction coefficient of multi-span continuous deck reinforced concrete (RC) bridges, isolated with single concave FPS devices, is analysed. The bridge is modelled through a six-degree-of-freedom (dof) system, where 5 dofs are

used to model the lumped masses of the pier and 1dof for the deck. The latter is considered infinitely rigid. Two FPS bearings are placed on top of the elastic RC pier and the rigid RC abutment, which is considered as a fixed support. The bridge is subjected to a set 40 of natural near fault records. Furthermore, many bridge models are considered by varying: the pier fundamental period, the ratio between the masses of the deck and the pier, the friction coefficient of the FPS devices and the ratio between the fundamental periods of the deck and of the ground motion. Nondimensional equation of motions have been solved such that the response becomes independent from the characteristic of the records, expressed in terms of peak ground acceleration-to-velocity ratio (PGA/PGV). The final result of this work is the computation of a linear regression in order to compute the nondimensional friction coefficient of the isolator as function of the deck period and the ground motion period, useful in the design phase of the FPS devices.

2 Bridge model and equations of motion

The seismic response of the bridge is evaluated by modelling a six-degree-of-freedom (dof) system, accounting for 5 dofs for the lumped masses of the pier and 1 additional dof to model the rigid RC deck. Previous studies have demonstrated that the use of 5 lumped masses to model the pier allows to obtain enough accuracy of the results avoiding larger computational efforts [13]-[14]. The friction pendulum system devices (FPS) are placed on top of the pier and the abutment, which is modelled as rigid and fixed. Fig. 1 shows the 6 dofs model adopted and their horizontal relative displacements.

When the structure is subjected to a seismic input, the equation of motion of the 6 dofs, evaluated along the horizontal direction, are:

$$
\begin{aligned}
&m_d\ddot{u}_d(t)+m_d\ddot{u}_{p5}(t)+m_d\ddot{u}_{p4}(t)+m_d\ddot{u}_{p3}(t)+m_d\ddot{u}_{p2}(t)+m_d\ddot{u}_{p1}(t)+c_d\dot{u}_d(t)+F_p(t)+F_a(t)=-m_d\ddot{u}_g(t)\\
&m_{p5}\ddot{u}_{p5}(t)+m_{p5}\ddot{u}_{p4}(t)+m_{p5}\ddot{u}_{p3}(t)+m_{p5}\ddot{u}_{p2}(t)+m_{p5}\ddot{u}_{p1}(t)-c_d\dot{u}_d(t)+c_{p5}\dot{u}_{p5}(t)+k_{p5}u_{p5}(t)-F_p(t)=-m_{p5}\ddot{u}_g(t)\\
&m_{p4}\ddot{u}_{p4}(t)+m_{p4}\ddot{u}_{p3}(t)+m_{p4}\ddot{u}_{p2}(t)+m_{p4}\ddot{u}_{p1}(t)-c_{p5}\dot{u}_{p5}(t)-k_{p5}u_{p5}(t)+c_{p4}\dot{u}_{p4}(t)+k_{p4}u_{p4}(t)=-m_{p4}\ddot{u}_g(t)\\
&m_{p3}\ddot{u}_{p3}(t)+m_{p3}\ddot{u}_{p2}(t)+m_{p3}\ddot{u}_{p1}(t)-c_{p4}\dot{u}_{p4}(t)-k_{p4}u_{p4}(t)+c_{p3}\dot{u}_{p3}(t)+k_{p3}u_{p3}(t)=-m_{p3}\ddot{u}_g(t)\\
&m_{p2}\ddot{u}_{p2}(t)+m_{p2}\ddot{u}_{p1}(t)-c_{p3}\dot{u}_{p3}(t)-k_{p3}u_{p3}(t)+c_{p2}\dot{u}_{p2}(t)+k_{p2}u_{p2}(t)=-m_{p2}\ddot{u}_g(t)\\
&m_{p1}\ddot{u}_{p1}(t)-c_{p2}\dot{u}_{p2}(t)-k_{p2}u_{p2}(t)+c_{p1}\dot{u}_{p1}(t)+k_{p1}u_{p1}(t)=-m_{p1}\ddot{u}_g(t)
\end{aligned}
\qquad (1a,b,c,d,e,f)
$$

where u_d is the deck displacement relative to the pier top, u_{pi} is the relative displacement of the ith lumped mass of the pier with respect to the lower one, m_d is the mass of the deck, m_{pi} is the mass of the ith lumped mass of the pier, while k_{pi} is the corresponding stiffness. The viscous damping coefficient for the device and for the pier masses are, respectively, c_d and c_{pi}; t is the instant of time and the dots are used to indicate differentiation. In the end, the resisting forces of the FPS bearings located on top of the abutment and on the pier are, respectively, $F_a(t)$ and $F_p(t)$. These forces can be expressed as the sum of an elastic component, coming from the pendular behaviour of the FPS device, and a viscous component, as follows [4]:

$$F_a(t) = \frac{m_d g}{2}\left[\frac{1}{R_a}\left(u_d(t) + \sum_{i=1}^{5} u_{pi}\right) + \mu_a\left(\dot{u}_d + \sum_{i=1}^{5}\dot{u}_{pi}\right)\mathrm{sgn}\left(\dot{u}_d + \sum_{i=1}^{5}\dot{u}_{pi}\right)\right]$$

$$F_p(t) = \frac{m_d g}{2}\left[\frac{1}{R_p}u_d(t) + \mu_p(\dot{u}_d)\mathrm{sgn}(\dot{u}_d)\right] \tag{2a,b}$$

where R_a and R_p are the radii of curvature of the FPS devices placed on the abutment and on the pier, respectively and assumed equal, the stiffness of the deck is computed as $k_d = W/R = m_d g/R$, half for the bearing on the abutment and half for the pier; g is the gravity constant; μ is the sliding friction coefficient of the bearings. It is noteworthy that the fundamental period of the deck can be expressed as $T_d = 2\pi\sqrt{m_d/k_d} = 2\pi\sqrt{R/\mathrm{g}}$, hence, it only depends on the geometrical property of the isolator (the radius of curvature), and not on the mass of the deck [4]. In literature [4],[6],[10],[15], many experimental evidences have emphasizes the dependence of the sliding friction coefficient on different parameters (e.g., sliding velocity, cumulative movements, temperature). In particular, the dependency of the sliding friction coefficient on the velocity is such that:

$$\mu(\dot{u}_d) = f_{\max} - (f_{\max} - f_{\min})\cdot\exp(-\alpha|\dot{u}_d|) \tag{3}$$

where $f_{\max}$ and $f_{\min}$ define, respectively, the sliding friction parameter at large and null velocity, α governs the transition from low to large velocities. Experimental results suggest to assume $f_{\max} = 3f_{\min}$ and $\alpha = 30$ [15].

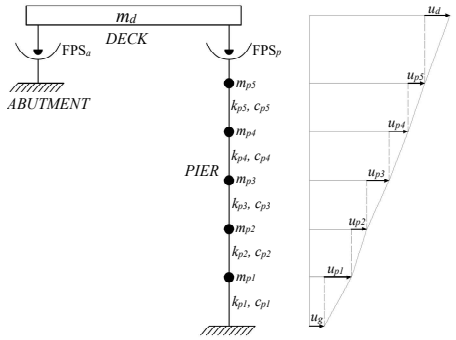

Fig. 1. Schematic representation of the six-degrees-of-freedom bridge model.

The equation of motions in (1) are then expressed in a nondimensional form, according to the Buckingham's Π-theorem, as illustrated in [16]-[18]. In particular, a time scale and a length scale are introduced and adopted for the nondimensionalization. In

this study, the former is represented by $1/\omega_g$, whit $\omega_g = 2\pi / T_g = PGA/PGV$ indicating the circular frequency of the ground motion and herein evaluated as the peak ground acceleration-to-velocity ratio. The latter is assumed as a_0 / ω_g^2, where a_0 is an intensity measure for the seismic input. The time scale is used to pass from the time t to $\tau = t\omega_g$ such that the ground motion input of equation (1) is expressed as:

$$\ddot{u}_g(t) = a_0 I(t) = a_0 \ell(\tau) \tag{4}$$

where $I(t)$ is a nondimensional function of the seismic input indicating its variation over the time t, while $\ell(\tau)$ contains the same information but in the time τ.

Finally, dividing the equations in (1) for the deck mass m_d and introducing the time and length scales, the equations in terms of nondimensional parameters are:

$$\ddot{\psi}_d(\tau)+\ddot{\psi}_{p5}(\tau)+\ddot{\psi}_{p4}(\tau)+\ddot{\psi}_{p3}(\tau)+\ddot{\psi}_{p2}(\tau)+\ddot{\psi}_{p1}(\tau)+2\xi_d\frac{\omega_d}{\omega_g}\dot{\psi}_d(\tau)+$$
$$+\left[\frac{1}{2}\frac{\omega_d^2}{\omega_g^2}\psi_d(\tau)+\frac{\mu_p(\dot{u}_d)g}{2a_0}\operatorname{sgn}(\dot{\psi}_d)\right]+$$
$$+\left[\frac{1}{2}\frac{\omega_d^2}{\omega_g^2}\left(\psi_d(\tau)+\sum\nolimits_{i=1}^{5}\psi_{pi}(\tau)\right)+\frac{g}{2a_0}\mu_a(\dot{u}_d+\sum_{i=1}^{5}\dot{u}_{pi})\left(\operatorname{sgn}\left(\dot{\psi}_d+\sum_{i=1}^{5}\dot{\psi}_{pi}\right)\right)\right]=-\ell(\tau)$$

$$\lambda_{p5}\left[\ddot{\psi}_{p5}(\tau)+\ddot{\psi}_{p4}(\tau)+\ddot{\psi}_{p3}(\tau)+\ddot{\psi}_{p2}(\tau)+\ddot{\psi}_{p1}(\tau)\right]-2\xi_d\frac{\omega_d}{\omega_g}\dot{\psi}_d(\tau)+2\xi_{p5}\frac{\omega_{p5}}{\omega_g}\lambda_{p5}\dot{\psi}_{p5}(\tau)+$$
$$+\lambda_{p5}\frac{\omega_{p5}^2}{\omega_g^2}\psi_{p5}(\tau)-\left[\frac{1}{2}\frac{\omega_d^2}{\omega_g^2}\psi_d(\tau)+\frac{\mu_p(\dot{u}_d)g}{2a_0}\operatorname{sgn}(\dot{\psi}_d)\right]=-\lambda_{p5}\ell(\tau)$$

$$\lambda_{p4}\left[\ddot{\psi}_{p4}(\tau)+\ddot{\psi}_{p3}(\tau)+\ddot{\psi}_{p2}(\tau)+\ddot{\psi}_{p1}(\tau)\right]-2\xi_{p5}\frac{\omega_{p5}}{\omega_g}\lambda_{p5}\dot{\psi}_{p5}(\tau)+2\xi_{p4}\frac{\omega_{p4}}{\omega_g}\lambda_{p4}\dot{\psi}_{p4}(\tau)+$$
$$-\lambda_{p5}\frac{\omega_{p5}^2}{\omega_g^2}\psi_{p5}(\tau)+\lambda_{p4}\frac{\omega_{p4}^2}{\omega_g^2}\psi_{p4}(\tau)=-\lambda_{p4}\ell(\tau)$$

$$\lambda_{p3}\left[\ddot{\psi}_{p3}(\tau)+\ddot{\psi}_{p2}(\tau)+\ddot{\psi}_{p1}(\tau)\right]-2\xi_{p4}\frac{\omega_{p4}}{\omega_g}\lambda_{p4}\dot{\psi}_{p4}(\tau)+2\xi_{p3}\frac{\omega_{p3}}{\omega_g}\lambda_{p3}\dot{\psi}_{p3}(\tau)-\lambda_{p4}\frac{\omega_{p4}^2}{\omega_g^2}\psi_{p4}(\tau)+$$
$$+\lambda_{p3}\frac{\omega_{p3}^2}{\omega_g^2}\psi_{p3}(\tau)=-\lambda_{p3}\ell(\tau)$$

$$\lambda_{p2}\left[\ddot{\psi}_{p2}(\tau)+\ddot{\psi}_{p1}(\tau)\right]-2\xi_{p3}\frac{\omega_{p3}}{\omega_g}\lambda_{p3}\dot{\psi}_{p3}(\tau)+2\xi_{p2}\frac{\omega_{p2}}{\omega_g}\lambda_{p2}\dot{\psi}_{p2}(\tau)-\lambda_{p3}\frac{\omega_{p3}^2}{\omega_g^2}\psi_{p3}(\tau)+$$
$$+\lambda_{p2}\frac{\omega_{p2}^2}{\omega_g^2}\psi_{p2}(\tau)=-\lambda_{p2}\ell(\tau)$$

$$\lambda_{p1}\ddot{\psi}_{p1}(\tau)-2\xi_{p2}\frac{\omega_{p2}}{\omega_g}\lambda_{p2}\dot{\psi}_{p2}(\tau)+2\xi_{p1}\frac{\omega_{p1}}{\omega_g}\lambda_{p1}\dot{\psi}_{p1}(\tau)-\lambda_{p2}\frac{\omega_{p2}^2}{\omega_g^2}\psi_{p2}(\tau)+\lambda_{p1}\frac{\omega_{p1}^2}{\omega_g^2}\psi_{p1}(\tau)=-\lambda_{p1}\ell(\tau)$$

(5a,b,c,d,e,f)

where $\psi_d = u_d \omega_g^2 / a_0$ and $\psi_{pi} = u_{pi} \omega_g^2 / a_0$ are the nondimensional displacements, $\omega_d = \sqrt{k_d / m_d}$ and $\omega_{pi} = \sqrt{k_{pi} / m_{pi}}$ are the circular vibration frequencies, $\xi_d = c_d / 2 m_d \omega_d$ and $\xi_{pi} = c_{pi} / 2 m_{pi} \omega_{pi}$ are the damping factors (respectively for the deck and for the i-th lamped masses of the pier) and $\lambda_p = \lambda_{pi} = m_{pi} / m_d$ is the mass ratio of the i-th lumped mass (assumed equal for all the lumped masses). Furthermore, the nondimensional parameters Π of the problem are:

$$\Pi_{\omega_p} = \frac{\omega_p}{\omega_d}, \quad \Pi_{\omega_g} = \frac{\omega_d}{\omega_g}, \quad \Pi_\lambda = \lambda_p, \quad \Pi_{\xi_d} = \xi_d, \quad \Pi_{\xi_p} = \xi_{pi}, \quad \Pi_\mu = \frac{\mu(\dot{u}_d) g}{a_0} \tag{6 a,b,c,d,e,f}$$

To discard the dependency of Π_μ on the velocity, we considered $\Pi_\mu^* = f_{\max} g / a_0$.

3 Parametric analysis

3.1 Ground motion records

According to the Performance Based Earthquake Engineering approach (PBEE) [19]-[20], the seismic intensity a_0 is represented by the parameter *PGA* (i.e., peak ground acceleration). Furthermore, a set of 40 near fault (NF) ground motion records is considered, with peak ground acceleration-to-velocity ratios between 0.21 and 0.97 (i.e., low ranges of PGA/PGV), magnitude between 6.19 and 7.62 and soil types B and C.

3.2 Deterministic parameters

The performance of the bridge isolated with FPS bearings is studied by including different values of the parameters involved in the problem. In particular, 2 pier periods are considered $T_p = 0.05s, 0.2s$, 15 period ratios in the range $T_d / T_g = 0.1 \div 1.6$, 3 mass ratios $\lambda_p = 0.1, 0.15, 0.3$ and 85 values for the nondimensional friction coefficient Π_μ^* between 0 and 1.5. The remaining parameters, i.e., Π_{ξ_d} and Π_{ξ_p} are set equal to 5% and 0% respectively [17],[21]-[24]. All the analyses have been solved in Matlab-Simulink [25]. To evaluate the performance of the bridge, the response parameter are chosen in terms of normalized relative peak displacement the pier (i.e., $\psi_{\mathrm{p,max}} = u_{\mathrm{p,max}} \omega_g^2 / a_0$) where the maximum pier response is intended as $u_{p,\max} = \left| \left(\sum_{i=1}^{5} u_{pi} \right) \right|_{\max}$. In the following, results are shown in terms of geometric mean (*GM*) and dispersion (β) of the response parameter *D* (i.e., $\psi_{\mathrm{p,max}}$) considering the lognormality of the data [17], [26]-[38] as follows:

$$GM(D) = \sqrt[N]{d_1 \cdot ... \cdot d_N};$$
$$\beta(D) = \sigma_{\ln}(D) = \sqrt{\frac{\left(\ln d_1 - \ln(GM)\right)^2 + ... + \left(\ln d_N - \ln(GM)\right)^2}{N-1}} \quad (7a,b)$$

where D is the generic response parameter, d_j is the j-th realization of the response parameter and $j=1,...,N$ with $N=40$ the total number of NF inputs. Then, the k-th percentile of the response parameter is given by $d_k = GM(D)\exp\left[f(k)\beta(D)\right]$, where $f(k)$ [39] is equal to 0, 1 and -1 for the 50th, 16th and 84th percentile, respectively.

4 Optimal sliding friction coefficient

The response parameter $\psi_{p,\max}$ corresponding to the normalized value of the maximum pier top displacement is illustrated in terms of geometric mean and dispersion as function of the normalized friction coefficient Π_{μ}^{*} and the ratio T_d / T_g for the two values of the pier fundamental periods T_p and the three quantity of λ_p. The geometric mean of the normalized response of the pier (Fig. 2a-b) increases for lower value of T_d / T_g since the lower the period of the deck, the larger are the forces acting on it and thus transmitted to the substructure. Furthermore, $GM(\psi_{p,\max})$ tends to decrease for larger values of the mass ratio. In addition, there is a slight decrease followed by an increase in the maximum normalized response of the pier top with the growth of the normalized friction coefficient, suggesting the evidence of an optimal value of Π_{μ}^{*} able to minimize the substructure response. Regarding the dispersion $\beta(\psi_{p,\max})$, the trend tends to slightly decrease in correspondence of the optimal value of the friction coefficient and turns out to be almost independent form the other parameters (Fig. 2c-d). The above mentioned considerations have resulted in the calculation of the optimal value for the normalized friction coefficient $\Pi_{\mu,opt}^{*}$ as function of the ratio T_d / T_g for the two values of T_p and the three quantity of λ_p, computed in terms of the 16th, 50th and 84th percentiles. In Fig.3 , the results corresponding to only the 50th percentile are shown. It can be noted that $\Pi_{\mu,opt}^{*}$ decreases with larger T_d / T_g ratios. Furthermore, Fig. 3 shows that there is not a large influence of both the pier fundamental period and the mass ratio in the computation of $\Pi_{\mu,opt}^{*}$. This suggests to perform a linear regression of the data to obtain the value of $\Pi_{\mu,opt}^{*}$ as only function of the parameter Π_{ω_g} as follows:

$$\Pi_{\mu,opt}^{*} = c_1 + c_2 \Pi_{\omega_g} \geq 0 \quad (8)$$

where the coefficients c_1 and c_2 together with the *R-squared* values are in Table 1.

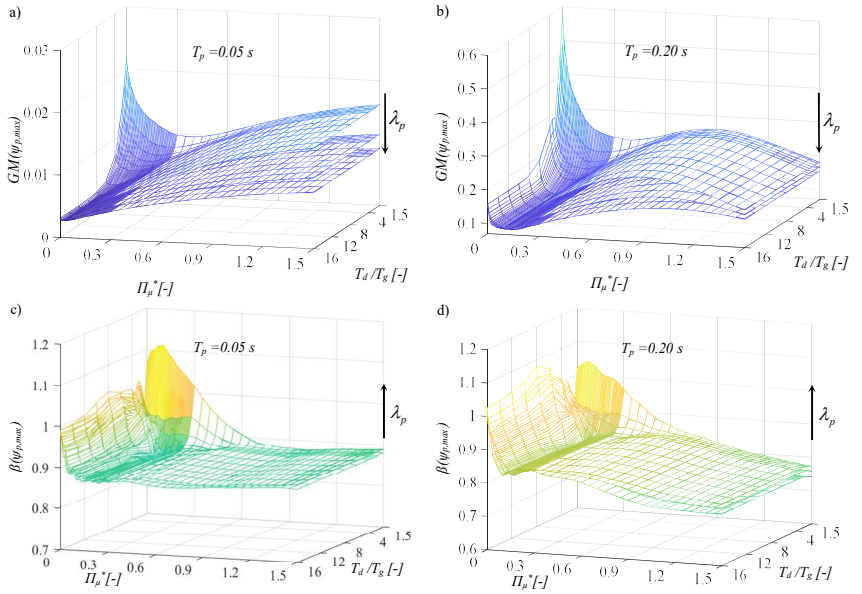

Fig. 2. Maximum normalized displacement of the pier top in terms of a-b) geometric mean and c-d) dispersion as function of Π_μ^* and T_d / T_g for $T_p = 0.05 - 0.2s$ and $\lambda_p = 0.1, 0.15, 0.2$.

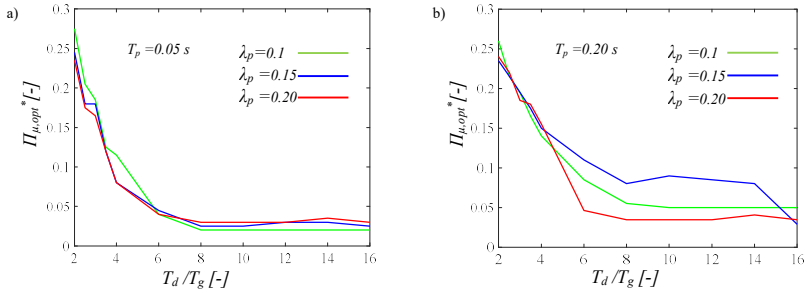

Fig. 3. Optimal value of the normalized friction coefficient as function of T_d / T_g for a) $T_p = 0.05s$ and b) $T_p = 0.2s$ and for the three values of $\lambda_p = 0.1, 0.15, 0.2$.

Table 1. Linear regression parameters for the optimal normalized friction coefficient

	50^{th}	16^{th}	84^{th}
R-squared	0.9292	0.8872	0.8588
c_1	-0.0093	-0.0130	0.0172
c_2	0.5430	0.5190	0.5069

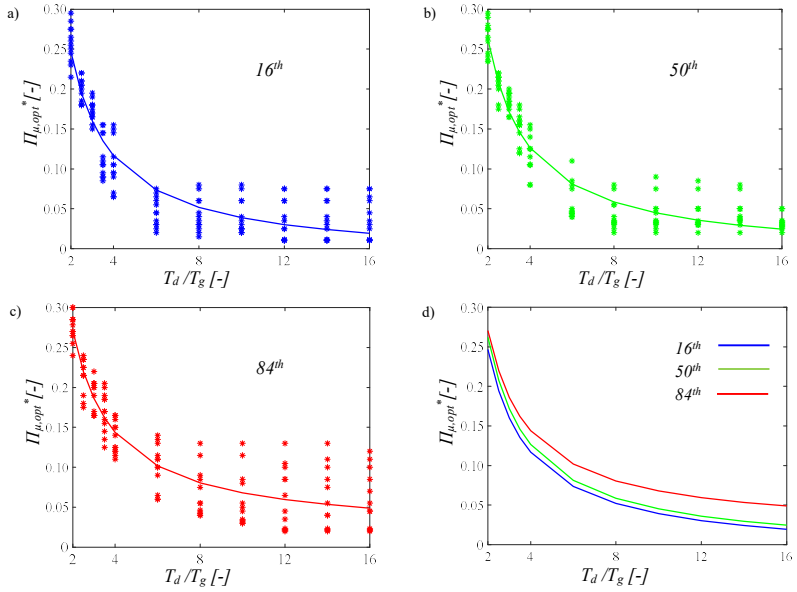

Fig. 4. Linear regression for the optimal value of the friction coefficient able at minimizing the a) 50th percentile b) 16th percentile and c) 84th percentile of the substructure response.

5 Conclusions

This study analyses the optimal value of the friction coefficient in case of seismic isolation of bridges with FPS devices. Many bridge models were considered within a parametric analysis. Then, each bridge model has been subjected to 40 near fault seismic records. The response of the substructure (i.e., the pier) has been evaluated in terms of nondimensional peak displacement normalized with respect to the ground motion characteristics through the acceleration-to-velocity (*PGA/PGV*) ratio. Results have shown the evidence of an optimal value of the friction coefficient able to minimize the substructure peak response. Hence, a linear regression of the data has led to an expression to compute the normalized optimal friction coefficient as function of the ratio between the fundamental period of the ground motion and of the deck.

References

1. Troisi, R., Alfano, G.: Towns as Safety Organizational Fields: An Institutional Framework in Times of Emergency. Sustainability 11, 7025 (2019). DOI:10.3390/su11247025.
2. Troisi R., Castaldo P., (2022) “Technical and organizational challenges in the risk management of road infrastructures”, Journal of Risk Research, 2022, DOI:10.1080/13669877.2022.2028884.

3. Ghobarah, A., Ali, H.M.: Seismic Performance of Highway Bridges. Engineering Structures 10(3), 157-66 (1988).
4. Zayas, V., Low, S., Mahin, S.: A simple pendulum technique for achieving seismic isolation. Earthquake Spectra 6(2), 317-333 (1990).
5. Su, L., Ahmadi, G., Tadjbakhsh, I.: Comparative Study of Base Isolation Systems. Journal of Engineering Mechanics 115(9), 1976-1992 (1989).
6. Mokha, A., Constantinou, M.C., Reinhorn, A.M.: Teflon Bearings in Base Isolation. I: Testing. Journal of Structural Engineering 116(2), 438-454 (1990).
7. Constantinou, M.C., Mokha, A., Reinhorn, A.M.: Teflon Bearings in Base Isolation. II: Modeling. Journal of Structural Engineering 116(2), 455-474 (1990).
8. Almazàn, J.L., De la Llera, J.C.: Physical model for dynamic analysis of structures with FPS isolators. Earthquake Engineering and Structural Dynamics 32(8), 1157–1184 (2003).
9. Mosqueda, G., Whittaker, A.S., Fenves, G.L.: Characterization and modeling of Friction Pendulum bearings subjected to multiple components of excitation. Journal of Structural Engineering 130(3), 433-442 (2004).
10. Jangid, R.S.: Computational numerical models for seismic response of structures isolated by sliding systems, Structural Control and Health Monitoring (12), 17–137 (2005).
11. Jangid, R.S.: Optimum frictional elements in sliding isolation systems. Computers and Structures 76(5), 651–661 (2000).
12. Jangid, R.S.: Optimum friction pendulum system for near-fault motions. Engineering Structures 27(3), 349–359 (2005).
13. Castaldo, P., Amendola, G.: Optimal Sliding Friction Coefficients for Isolated Viaducts and Bridges: A Comparison Study. Structural Control and Health Monitoring 28(12), (2021).
14. Castaldo, P., Amendola, G.: Optimal DCFP bearing properties and seismic performance assessment in nondimensional form for isolated bridges. Earthquake Engineering and Structural Dynamics 50(9), 2442–2461 (2021).
15. Constantinou, M.C., Whittaker, A.S., Kalpakidis, Y., Fenz, D.M., Warn, G.P.: Performance of Seismic Isolation Hardware Under Service and Seismic Loading. Technical Report MCEER-07-0012, (2007).
16. Makris, N., Black, C.J.: Dimensional analysis of inelastic structures subjected to near fault ground motions. Technical report: EERC 2003/05. Berkeley: Earthquake Engineering Research Center, University of California, (2003).
17. Castaldo, P, Tubaldi, E.: Influence of FPS bearing properties on the seismic performance of base-isolated structures. Earthquake Engineering and Structural Dynamics 44(15), 2817–2836 (2015).
18. Castaldo, P., Tubaldi, E.: Influence of Ground Motion Characteristics on the Optimal Single Concave Sliding Bearing Properties for Base-isolated Structures. Soil Dynamics and Earthquake Engineering 104, 346-64 (2018).
19. Aslani, H., Miranda, E.: Probability-based seismic response analysis. Engineering Structures 27(8), 1151-1163 (2005).
20. Porter, K.A.: An overview of PEER's performance-based earthquake engineering methodology. In: Proceedings of the 9th International Conference on Application of Statistics and Probability in Civil Engineering, ICASP9, San Francisco, California, (2003).
21. De Iuliis, M., Castaldo, P.: An energy-based approach to the seismic control of one-way asymmetrical structural systems using semi-active devices. Ingegneria Sismica-International Journal of Earthquake Engineering 29(4), 31-42 (2012).
22. Castaldo, P., De Iuliis, M.: Optimal integrated seismic design of structural and viscoelastic bracing-damper systems. Earthquake Engineering and Structural Dynamics 43(12), 1809–1827 (2014).

23. Castaldo, P., Palazzo, B., Ferrentino, T., Petrone, G.: Influence of the strength reduction factor on the seismic reliability of structures with FPS considering intermediate PGA/PGV ratios. Composites Part B: Engineering 115, 308-315 (2017).
24. Castaldo, P., Palazzo, B., Ferrentino, T.: Seismic reliability-based ductility demand evaluation for inelastic base-isolated structures with friction pendulum devices. Earthquake Engineering and Structural Dynamics 46(8), 1245-1266 (2017).
25. Math Works Inc. MATLAB-High Performance Numeric Computation and Visualization Software. User's Guide. Natick (MA) USA (1997).
26. Troisi, R., Alfano, G.: Firms'crimes and land use in Italy. An exploratory data analysis. Smart Innovation, Systems and Technologies 178 SIST, 749–758 (2020).
27. Garzillo, C., Troisi, R.: Le decisioni dell'EMA nel campo delle medicine umane. In EMA e le relazioni con le Big Pharma - I profili organizzativi della filiera del farmaco. G. Giappichelli, 85-133 (2015).
28. Golzio, L.E., Troisi, R.: The value of interdisciplinary research: a model of interdisciplinarity between legal re-search and research in organizations. Journal For Development And Leadership 2, 23-38 (2013).
29. Nese, A., Troisi R.: Corruption among mayors: evidence from Italian Court of Cassation judgments. Trends In Organized Crime 22(3), 298-323 (2019).
30. Troisi, R., Golzio, L.E.: Legal studies and organization theory: a possible cooperation. In: 16th EURAM Conference Manageable cooperation. European Academy of Management, Paris, 1-4 June (2016).
31. Troisi, R., Guida, V.: Is the Appointee Procedure a Real Selection or a Mere Political Exchange? The Case of the Italian Health-Care Chief Executive Officers. Journal of Entrepreneurial and Organizational Diversity 7 (2), 19-38 (2018). DOI:10.5947/jeod.2018.008.
32. Troisi, R.: Le risorse umane nelle BCC: lavoro e motivazioni al lavoro. Progetto aree bianche. Il sistema del credito cooperativo in Campania 1, 399-417 (2012).
33. Nesticò, A., Moffa, R. (2018). Economic analysis and Operational Research tools for estimating productivity levels in off-site construction [Analisi economiche e strumenti di Ricerca Operativa per la stima dei livelli di produttività nell'edilizia off-site], Valori e Valutazioni n. 20, pp. 107-128, ISSN: 2036-2404. DEI Tipografia del Genio Civile, Roma.
34. Nesticò, A., Maselli, G. (2020). Declining discount rate estimate in the long-term economic evaluation of environmental projects. Journal of Environmental Accounting and Management, Vol. 8, Issue 1, pp. 93-110. https://doi.org/10.5890/JEAM.2020.03.007.
35. Castaldo P., Gino D., Marano G., Mancini G. (2022) "Aleatory uncertainties with global resistance safety factors for non-linear analyses of slender reinforced concrete columns", Engineering Structures, 2022, 255, 113920, S0141-0296(22)00078-5.
36. Troisi, R., Alfano, G.: Is regional emergency management key to containing COVID-19? A comparison between the regional Italian models of Emilia-Romagna and Veneto. International Journal of Public Sector Management, (2021). DOI: 10.1108/IJPSM-06-2021-0138.
37. Troisi, R., Di Nauta, P., Piciocchi, P.: Private corruption: An integrated organizational model. European Management Review, (2021).
38. Nese, A., Troisi, R.: Individual Preferences and Job Characteristics: An Analysis of Cooperative Credit Banks. Labour 28(2), 233–249 (2014).
39. Ang, A.H.S., Tang, W.H.: Probability Concepts in Engineering-Emphasis on Applications to Civil and Environmental Engineering. John Wiley & Sons, New York USA (2007).